Improving reliability of heat and fluid flow calculation during conduction mode laser spot welding by multivariable optimisation

A. De*[1] and T. DebRoy[2]

Several uncertain parameters affect the reliability of heat transfer and fluid flow calculations during conduction mode laser spot welding because their values cannot be prescribed from fundamental principles. These parameters include absorptivity of the laser beam, effective thermal conductivity and effective viscosity of liquid metal in the weld pool. Values of these parameters are usually adjusted by trial and error so that the computed results agree with the corresponding experimental values. Here it is shown that by integrating multivariable constrained optimisation with convective heat transfer and fluid flow calculations, the values of the uncertain parameters can be obtained from a limited volume of experimental data. The optimisation technique requires numerically calculated sensitivity values of weld dimensions with respect to absorptivity, effective thermal conductivity and effective viscosity and minimises the discrepancy between the predicted and the measured weld dimensions. The numerical heat transfer and fluid flow model embodying the optimised values of the uncertain parameters could accurately compute values of weld dimensions for new welding conditions. Reliability of heat transfer and fluid flow calculations can be significantly enhanced by determining the values of uncertain parameters from a limited volume of experimental data using a multivariable optimisation technique with a numerical heat transfer and fluid flow model.

Keywords: Laser beam welding, Heat transfer, Fluid flow, Conduction mode, Multivariable optimisation

Introduction

Numerical calculations of heat transfer and fluid flow during fusion welding have been used to calculate peak temperature, weld thermal cycle, cooling rate and weld pool geometry.[1–6] The computed thermal cycles have been used for offline estimation of weld metal phase composition,[7–13] grain structure,[14] topology,[15] inclusion structure,[16–18] solute concentration[19] and weld metal composition change owing to both vaporisation of alloying elements[20,21] and dissolution of gases.[22,23] These calculations have enabled detailed understanding of physical processes during spot welding[24,25] and complex weld joint geometry.[26–30] The equations of conservation of mass, momentum and energy provide a reliable phenomenological description of the physical processes in the weld pool. However, transport phenomena based numerical models of weld pool are not widely used for designing and manufacturing purposes. There are several reasons for the restricted use of these powerful models. An important difficulty is that all the necessary input variables cannot be prescribed accurately from fundamental principles. The reliability of the numerical solution of the transport phenomena based models are affected by the uncertainty in the values of several input parameters.

Many input parameters for numerical simulation of a conduction mode laser spot welding can be easily specified. These include beam power, focused beam diameter and thermophysical properties of the material being welded. However, a reliable value of absorptivity cannot be specified apriori because it depends on the surface finish of the specimen, mode of welding, i.e. keyhole or conduction mode, and the temperature distribution on the weld pool.[31] An accurate value of absorptivity is needed for the calculation of the rate of heat absorption by the substrate. Similarly, the values of effective thermal conductivity and effective viscosity of weld pool are difficult to specify without solving additional partial differential equations.[32–34] The two equation k–ε turbulence model is sometimes used for the estimation of the effective viscosity and effective thermal conductivity in the weld pool.[32–34] However, the k–ε turbulence model contains several empirical constants that were originally estimated to model parabolic fluid flow in large systems. Their applicability for strongly elliptic recirculating flows in very small weld pools has never been rigorously examined. Furthermore, the use of a turbulence model significantly increases the volume and complexity of computations. Appropriate values of

[1]Mechanical Engineering Department, IIT Bombay, Mumbai 400 076, India
[2]Department of Material Science and Engineering, The Pennsylvania State University, University Park, PA, USA

*Corresponding author, email amit@me.iitb.ac.in

Published by Maney on behalf of the Institute
Received 11 September 2005; accepted 24 October 2005
DOI 10.1179/174329306X84346

effective thermal conductivity and effective viscosity provide a practical recourse for reliable modelling of the high rates of transport of heat, mass and momentum in weld pools with strong fluctuating velocities.

Because the effective thermal conductivity and viscosity are system properties,[32–34] their values and the uncertain value of absorptivity are determined in the present work from a limited volume of measured weld pool dimensions for conduction mode laser spot welding[35] utilising an optimisation algorithm and a numerical heat transfer and fluid flow model. The optimisation algorithm minimises the error between the predicted and the experimentally observed penetrations and the weld widths by tracking the sensitivity of the computed weld pool dimensions on the values of absorptivity, effective thermal conductivity and effective viscosity. The sensitivity terms are calculated by running the heat transfer and fluid flow model several times for each measurement considering small changes in the absorptivity, effective thermal conductivity and effective viscosity.[36,37] Although similar efforts related to weld pool characteristics have been reported in the recent past,[38–42] the present work differs from the previous work in an important issue. In the optimisation work reported here, an important constraint is that the model inputs and the outputs are related through the phenomenological laws of conservation of mass, momentum and energy. Not only do the solutions confirm to the reality of experiments, but also they obey the phenomenological laws.

Heat transfer and fluid flow simulation

The movement of molten metal in weld pool in three-dimensional Cartesian coordinate system is represented by the following momentum conservation equation[43]

$$\rho\frac{\partial u_j}{\partial t}+\rho\frac{\partial(u_i u_j)}{\partial x_i}=\frac{\partial}{\partial x_i}\left(\mu\frac{\partial u_j}{\partial x_i}\right)+S_j \tag{1}$$

where ρ is the density, t the time, x_i the distance along the i=1, 2 and 3 directions, u_j the velocity component along the j direction, μ the effective viscosity and S_j the source term for the jth momentum equation and is given as[25,44]

$$S_j=\frac{\partial p}{\partial x_j}+\frac{\partial}{\partial x_j}\left(\mu\frac{\partial u_j}{\partial x_j}\right)-C\left[\frac{(1-f_L)^2}{f_L^3+B}\right]u_j+Sb_j \tag{2}$$

where p is the pressure, f_L the liquid fraction, B a constant introduced to avoid division by 0 and C ($=1{\cdot}6\times10^4$) a constant that takes into account mushy zone morphology and Sb_j represents both the electromagnetic and buoyancy source terms. The third term on the right hand side (RHS) represents the frictional dissipation in the mushy zone according to the Carman–Kozeny equation for flow through a porous medium.[45,46] The pressure field was obtained by solving the following continuity equation simultaneously with the momentum equation

$$\frac{\partial(\rho u_i)}{\partial x_i}=0 \tag{3}$$

the total enthalpy H is represented by a sum of sensible heat h and latent heat content ΔH, i.e. $H=h+\Delta H$ where $h=\int C_p dT$, C_p is the specific heat, T is the temperature and $\Delta H=f_L L$ where L is the latent heat of fusion and the liquid fraction f_L is assumed to vary linearly with temperature in the mushy zone[47]

$$f_L=\begin{cases}1 & T>T_L\\ \frac{T-T_S}{T_L-T_S} & T_S\leqslant T\leqslant T_L\\ 0 & T<T_S\end{cases} \tag{4}$$

where T_L and T_S are the liquidus and solidus temperature, respectively. The thermal energy transport in the weld workpiece can be expressed by the following modified energy equation[25,47]

$$\rho\frac{\partial h}{\partial t}+\rho\frac{\partial(u_i h)}{\partial x_i}=\frac{\partial}{\partial x_i}\left(\frac{k}{C_p}\frac{\partial h}{\partial x_i}\right)-\rho\frac{\partial(\Delta H)}{\partial t}-\rho\frac{\partial(u_i\Delta H)}{\partial x_i} \tag{5}$$

where k is the thermal conductivity. The effective thermal conductivity in the liquid weld pool is also a property of the specific welding system and not a fundamental property of the liquid metal. Therefore, the value of the effective thermal conductivity is not known. Because the weld is symmetrical about the weld centreline, only half of the workpiece is considered. The weld top surface is assumed to be flat. The velocity boundary condition is given as[47]

$$\begin{aligned}\mu\frac{\partial u}{\partial z}&=f_L\frac{d\gamma}{dT}\frac{\partial T}{\partial x}\\ \mu\frac{\partial v}{\partial z}&=f_L\frac{d\gamma}{dT}\frac{\partial T}{\partial y}\\ w&=0\end{aligned} \tag{6}$$

where u, v and w are the velocity components along the x, y and z directions, respectively, γ is the surface tension and T is the temperature. The w velocity is 0 because the liquid metal is not transported across the weld pool top surface. The heat flux at the top surface is given as

$$k\frac{\partial T}{\partial z}=\frac{dP\eta}{\pi r_b^2}\exp\left[-\frac{d(x^2+y^2)}{r_b^2}\right]-\sigma\varepsilon(T^4-T_a^4)-h_c(T-T_a) \tag{7}$$

where r_b is the laser beam radius, d the beam distribution factor, P the laser beam power, η the absorptivity, σ the Stefan–Boltzmann constant, h_c the heat transfer coefficient and T_a the ambient temperature. The first term on the right hand side is the heat input from the heat source, defined by a Gaussian heat distribution. The second and third terms represent the heat loss by radiation and convection, respectively. The boundary conditions are defined as zero flux across the symmetric surface (i.e. at y=0) as[25,47]

$$\frac{\partial u}{\partial y}=0,\quad v=0,\quad \frac{\partial w}{\partial y}\quad\text{and}\quad\frac{\partial h}{\partial y}=0 \tag{8, 9}$$

at all other surfaces, temperatures are taken as ambient temperature and the velocities are set to 0.

In order to investigate the combined effects of laser power, spot diameter and substrate thermophysical properties, a unified non-dimensional heat input index N_{HI} is constituted as

$$N_{HI}=\frac{\left(\frac{P}{\pi r_b^2}\right)(t_{on})\left(\frac{1}{d}\right)}{\rho C_{PS}(T_L-T_a)+\rho L} \tag{10}$$

where P is the laser power (W), r_b the spot radius (m),

Table 1 Measured weld dimensions, welding parameters[35] and heat input index

Data set index	Laser power, W	Spot radius, mm	Laser on-time, s	N_{HI}	Weld penetration, mm	Weld width, mm
1	1900	1·40	5·0	5·87	0·60	2·20
2	3500	1·40	15·0	32·44	1·50	4·20
3	3850	1·40	5·0	11·89	1·10	4·00
4	5000	1·10	15·0	75·04	1·83	5·50
5	5200	1·40	5·0	16·06	1·45	5·30
6	5200	1·35	15·0	51·84	1·75	5·50

Table 2 Chemical composition of steel used for welding experiments (for data set index 1, 3, 4, 5 and 6),[35] wt-%

C	Cr	W	Mo	V	Co	Mn	Si	S	O	Ti	N	Al	Fe
0·87	3·89	6·36	4·87	1·80	4·57	0·24	0·53	0·002	0·0049	<0·01	0·032	<0·005	Bal.

t_{on} the laser on-time (s), d the substrate thickness (m), α the thermal diffusivity ($m^2\ s^{-1}$), ρ the density ($kg\ m^{-3}$), C_{PS} the specific heat of the solid metal ($J\ kg^{-1}\ K^{-1}$), L the latent heat of fusion ($J\ kg^{-1}$) and T_L and T_a are the liquidus and ambient temperatures (K), respectively. In equation (1), the numerator can be considered as the total incident laser power per unit volume. The denominator depicts the enthalpy required to heat a unit volume of metal from ambient temperature to liquidus temperature. It can be noted that the expression $P/\pi r_b^2$ in the numerator of equation (1), when multiplied by the absorptivity η, will depict the actual absorbed heat flux.

Table 1 depicts six sets of measurements of weld dimensions and the corresponding welding parameters that have been used in the present investigation. The chemical compositions of the steels used are presented in Tables 2 and 3. The thermophysical properties of steel are given in Table 4. The optimised values of absorptivity, effective thermal conductivity and effective viscosity were tested by comparing the computed weld dimensions with the corresponding experimentally determined values for welding conditions different from those used in the optimisation.

Optimisation procedure

The goal of the optimisation process is to determine the three important uncertain parameters which are laser beam absorption coefficient, effective thermal conductivity and effective viscosity. It is difficult to optimise more than two parameters by trial and error. Furthermore, commercial optimisation programs are also not appropriate for the current problem for two reasons. First, the necessary coupling of a commercial software with a three-dimensional heat transfer and fluid flow code is not a trivial task. Second, the contents of the commercial codes are often not adequately disclosed. In contrast, the coupling of a gradient based optimisation technique with a heat transfer and fluid flow code is straightforward and the use of this optimisation technique does not suffer from the lack of transparency of the commercial codes.

The Levenberg–Marquardt (LM) method which is a gradient based multivariable optimisation technique has been used in the work reported here. A detailed description of this technique is available[39–42] in the literature and is not repeated here. Only its specific application of the determination of absorptivity, effective thermal conductivity and effective viscosity are discussed in brief. An objective function embodying the difference between the computed and the measured values of weld dimensions is minimised. Because the weld dimensions are linked with the values of the absorptivity, effective thermal conductivity and effective viscosity, their values affect the objective function. The search for the optimised values of unknown parameters follows the direction of the objective function gradient with step size modification by an adjustable parameter in subsequent iterations.[48–51] The objective function O(f)

Table 3 Chemical composition of steel used for welding experiments (for data set index 4),[35] wt-%

C	Cr	W	Mo	V	Co	Mn	Si	S	O	Ti	N	Al	Fe
0·90	3·89	6·30	4·87	1·77	3·89	0·23	0·32	0·008	0·0035	<0·005	0·032	0·015	Bal.

Table 4 Data used for calculations of temperature and velocity fields[35]

Physical property	Value
Liquidus temperature T_L, K	1630·0
Solidus temperature T_S, K	1620·0
Ambient temperature T_a, K	293·0
Density of liquid metal ρ, $kg\ m^{-3}$	8100·0
Thermal conductivity of solid k_S, $W\ m^{-1}\ K^{-1}$	25·08
Thermal conductivity of liquid k_L $W\ m^{-1}\ K^{-1}$	25·08
Specific heat of solid C_{PS}, $J\ kg^{-1}\ K^{-1}$	627·0
Specific heat of liquid C_{PL} $J\ kg^{-1}\ K^{-1}$	723·0
Enthalpy of solid at melting point, $kJ\ kg^{-1}$	1045·0
Enthalpy of liquid at melting point, $kJ\ kg^{-1}$	1315·0
Temperature coefficient of surface tension $d\gamma/dT$, $N\ m^{-1}\ K^{-1}$	$-0{\cdot}5 \times 10^{-3}$
Coefficient of thermal expansion β, K^{-1}	$1{\cdot}0 \times 10^{-5}$
Viscosity of molten iron at 1823 K μ_{fl}, $kg\ m^{-1}\ s^{-1}$	$6{\cdot}7 \times 10^{-3}$

is defined as

$$O(f)=\sum_{m=1}^{M}\left(\frac{p_m^c-p_m^{obs}}{p_m^{obs}}\right)^2+\sum_{m=1}^{M}\left(\frac{w_m^c-w_m^{obs}}{w_m^{obs}}\right)^2$$
$$=\sum_{m=1}^{M}\left(p_m^*-1\right)^2+\sum_{m=1}^{M}\left(w_m^*-1\right)^2 \quad (11)$$

where p_m^c and w_m^c are the penetration and the width of the weld pool computed by the numerical heat transfer and fluid flow model, respectively and p_m^{obs} and w_m^{obs} are the corresponding measurements at similar welding conditions. p_m^* and w_m^* are non-dimensional penetration and weld width defined by equation (11). In equations (11), the subscript m refers to a specific weld in a series of M number of total welds and f corresponds to the given set of three unknown parameters in non-dimensional forms as

$$\{f\}\equiv\{f_1 \quad f_2 \quad f_3\}\equiv\{k^* \quad \mu^* \quad \eta\}$$
$$\equiv\left\{\frac{k_{eff}}{k_S} \quad \frac{\mu}{\mu_{fl}} \quad \eta\right\} \quad (12)$$

where k_S, μ_{fl}, k_{eff}, μ and η are thermal conductivity of solid material at room temperature, viscosity of molten iron at 1823 K, effective thermal conductivity, effective viscosity of liquid metal and absorptivity, respectively. Assuming that O(f) is continuous and has a minimum value, the LM method tries to obtain the optimum values of f_1, f_2 and f_3 by minimising O(f) with respect to them. In other words, equation (11) is differentiated with respect to f_1, f_2 and f_3, and each derivative is made equal to 0 as

$$\left[\frac{\partial O(f)}{\partial f_i}\right]_{i=1,3}= \quad (13)$$
$$2\left[\sum_{m=1}^{M}\left(p_m^*-1\right)\frac{\partial p_m^*}{\partial f_i}+\sum_{m=1}^{M}\left(w_m^*-1\right)\frac{\partial w_m^*}{\partial f_i}\right]_{i=1,3}=0$$

where f_i represents k^*, μ^* or η. The variables p_m^c and w_m^c in equation (13) are obtained from the numerical heat transfer and fluid flow calculations for a certain set of f_1, f_2 and f_3, i.e. k^*, μ^* and η. The partial derivatives in equation (13) are defined as the sensitivity of the computed weld width and penetration with respect to the unknown parameters and these are computed numerically. For example, the sensitivity of p_m^* with respect to f_1 is calculated as

$$\frac{\partial p_m^*}{\partial f_1}= \quad (14)$$
$$\left[\begin{matrix}p_m^*(f_1+\delta f_1, f_2, f_3, \text{other known parameters})-\\ p_m^*(f_1, f_2, f_3, \text{other known parameter})\end{matrix}\right]/\delta f_1$$

where δf_1 is very small compared with f_1. The solution of equation (13) is achieved when the calculated values of p_m^c and w_m^c are close to the corresponding measured values of p_m^{obs} and w_m^{obs}, i.e. both $p_m^*$and w_m^* become close to one for all M welds. Equation (13) does not explicitly contain f_1, f_2 and f_3. Therefore, equation (13) is rearranged so that it can serve as a basis for an iterative scheme to evaluate the optimum values of f_1, f_2 and f_3. The procedure is explained in the Appendix. The final form of equations to be solved is

$$[S]\{\Delta f^k\}=-\{S^*\} \quad (15)$$

$$\text{where } \{f_i^{k+1}\}=\{f_i^k\}+\{\Delta f_i^k\} \text{ for } i=1,3 \quad (16)$$

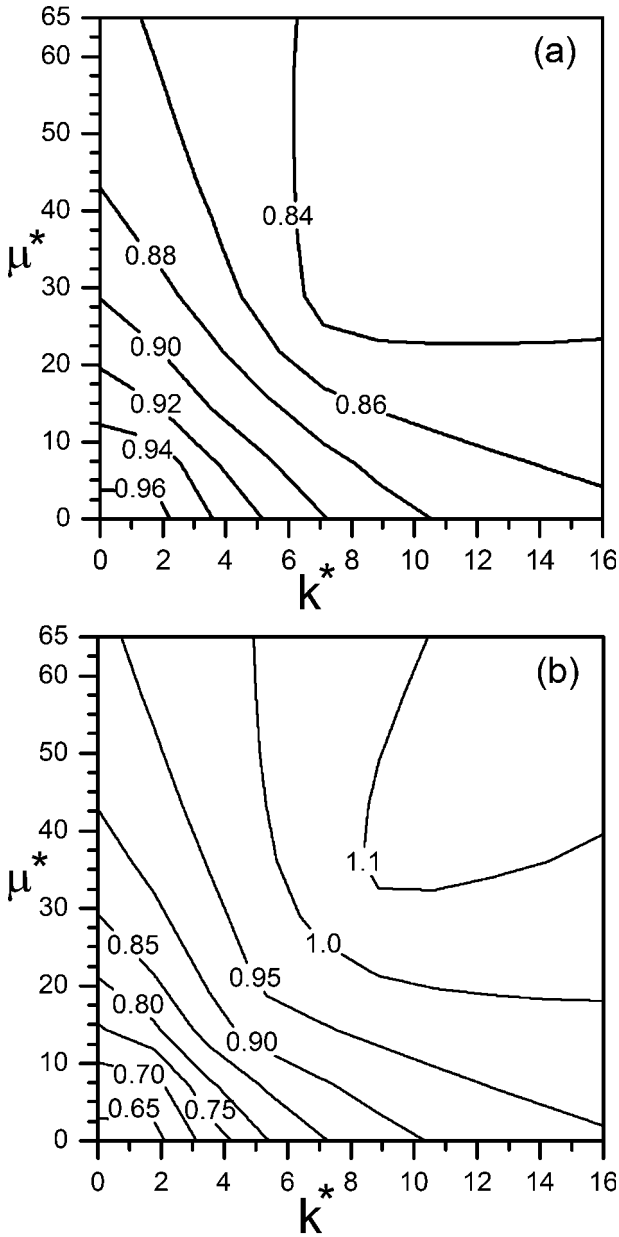

1 Influence of k^* and μ^* on *a* p_m^* and *b* w_m^* with assumed absorptivity η as 0·10: welding parameters P=3850 W, r_b=1·4 mm and laser on-time=5·0 s

and $\{f_i^{k+1}\}$ refers to the three unknown increments after $(k+1)$th iteration. Equation (15) provides the solution of the three unknown increments, $\{\Delta f_i^k\}$ corresponding to the three unknown parameters. Furthermore, a manual damping factor is used that continually tracks the search step (or increment) so that the optimal solution cannot move away from the last computed minimum value of the objective function.

Results and discussion

Obtaining the optimum solutions of the three unknown parameters requires the computation of a set of sensitivity terms S_{ij} defined by equation (42). These terms depict the influence of variation of the unknown variables on the dimensionless penetration and weld width. Figure 1*a* and *b* depicts a number of isocontours of the dimensionless width w_m^* and penetration p_m^* as a function of k^* and μ^* for η=0·10 corresponding to data

set #3 in Table 1. Figure 1*a* shows that w_m^* decreases with increasing k^* and/or μ^* and Fig. 1*b* depicts that p_m^* decreases with decreasing k^* and/or μ^*. When both p_m^* and w_m^* are 1, p_m^c equals to p_m^{obs} and w_m^c equals to w_m^{obs}, and the calculated results agree with the corresponding measured values. A comparison of Fig. 1*a* and *b* reveals that smaller values of k^* and μ^* favour better prediction for weld width while greater values of k^* and μ^* tend to provide more reliable prediction for penetration. The penetration p_m^c increases with k^* because high values of thermal conductivity facilitate rapid heat transport in the downward direction. However, the higher thermal conductivity also reduces the surface temperature gradient and the radial convective heat transport and consequently, w_m^c decreases. Higher values of μ^* lowers radial convection and the convective heat flow resulting in higher peak temperature and smaller value of w_m^c. The higher peak temperature also enhances downward heat conduction and increases p_m^c. In addition, as k^* is progressively increased, conduction becomes the dominant mechanism of heat transfer and changes in μ^* do not significantly alter either the peak temperature or the convective heat transfer rate. Therefore, the computed weld pool dimensions do not change significantly with μ^* at high values of k^* as observed in Fig. 1*a* and *b*. It should be noted that for a particular measurement, p_m^{obs} and w_m^{obs} remain the same while the predicted values of weld dimensions, i.e. p_m^c and w_m^c, vary as the values of k^* or μ^* change, thereby changing the values of p_m^* and w_m^*.

In addition to the variation in k^* or μ^*, change in the absorption coefficient η will also influence the computed values of weld width and penetration presented in Fig. 1*a* and *b*. An increase in η implies greater amount of absorbed heat flux [equation (8)] by substrate leading to higher peak temperature and temperature gradient, and larger computed weld pool dimensions for a specific set of k^* and μ^*. In contrast, a decrease in η will tend to smaller values of peak temperature and computed weld pool dimensions for a specific set of k^* and μ^*. Such combined influences of k^*, μ^* and η on computed weld dimensions are presented next in Figs 2 and 3. The results show the dependence of the objective function O(f) [equation (11)] on k^* and μ^* respectively for η=0·10, 0·13 and 0·18 corresponding to data set #4 in Table 1. It should be noted that O(f) denotes the error in prediction of weld dimensions in non-dimensional form. Three points are worth noting in Fig. 2*a–c*. First, with increasing η, lesser values of k^* and μ^* tend to reduce the value of O(f) although the minimum achievable value of O(f) will depend on the specific η. Second, for a specific combination of k^* and μ^*, the value of O(f) can vary considerably for small change in η. Lastly, corresponding to this specific welding condition, the most suitable value of η appears to lie around 0·13 (Fig. 2*b*). The influence of η along with k^* and μ^* on O(f) is possible to explain. For a particular beam power density and specific combination of k^* and μ^*, an increase in η simply increases the absorbed heat flux by the substrate and therefore, the computed weld dimensions will increase. In contrast, a decrease in η reduces the absorbed heat flux by the substrate and therefore, the values of the computed weld dimensions will decrease. In both cases, because p_m^* and w_m^* deviate from their target unit values, the value of O(f) will increase.

Figure 2*a–c* also includes a straight line that needs further attention. Consider an isocontour of the objective

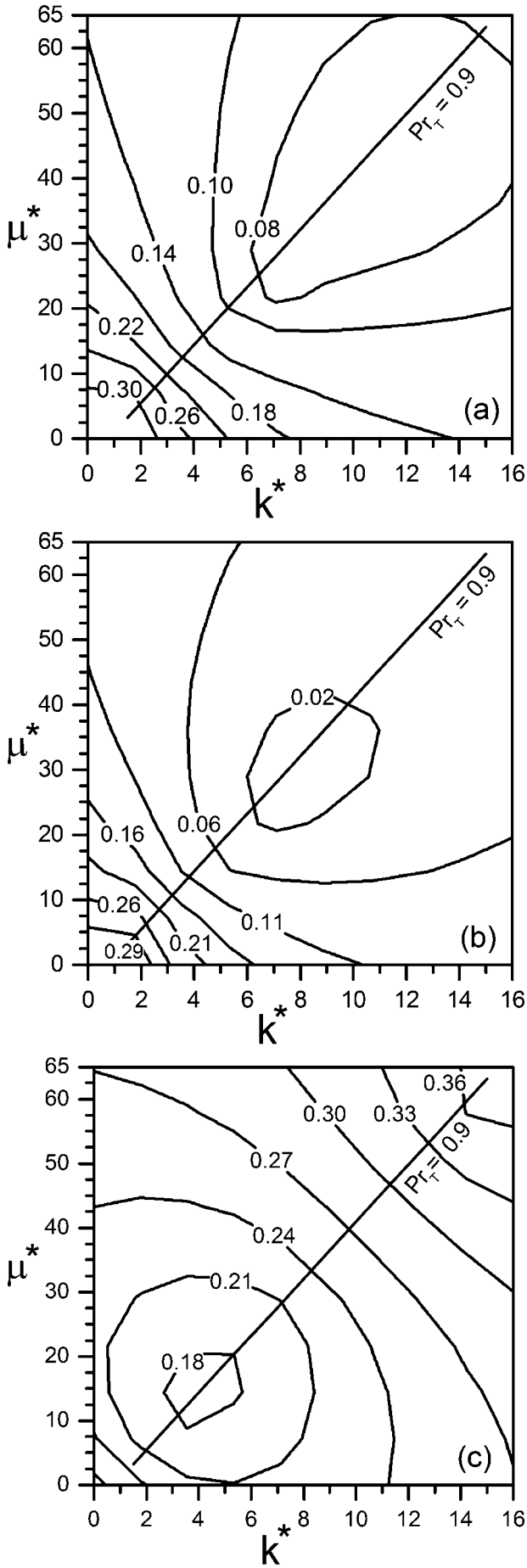

2 Influence of k^* and μ^* on O(f) for absorptivity η values as *a* 0·10, *b* 0·13 and *c* 0·18: welding parameters P=5000 W, r_b=1·1 mm and laser on-time=15·0 s

function with a value of 0·02 in Fig. 2*b*. Graphically, this contour indicates that a number of combinations of k^* and μ^* can lead to satisfactory numerical prediction of weld dimensions, $O(f)=0{\cdot}02$, when $\eta=0{\cdot}13$. However, because there are multiple solutions, a specific combination must be chosen from many possibilities. Furthermore, a physically meaningful choice needs to be made. A helpful constraint is the commonly accepted value of turbulent Prandtl number defined as

$$Pr_{\mathrm{T}} = \frac{\mu_{\mathrm{T}} C_{\mathrm{PL}}}{k_{\mathrm{T}}} \tag{17}$$

where $\mu_{\mathrm{eff}}=\mu_{\mathrm{fl}}+\mu_{\mathrm{T}}$ and $k_{\mathrm{eff}}=k_{\mathrm{L}}+k_{\mathrm{T}}$; μ_{T} and k_{T} are the turbulent viscosity and thermal conductivity that can be considered to be accounting for the fluctuating fluid velocity within the weld pool. Because Pr_{T} is commonly[24–25] prescribed as 0·9, Fig. 2*a–c* includes a dashed line corresponding to $Pr_{\mathrm{T}}=0{\cdot}9$ and the most suitable value of k^* and μ^* would allow $O(f)$ to remain close to the dashed line.

Figure 3*a–c* shows the influence of k^* and μ^* on the objective function $O(f)$ for three values of η =0·10, 0·13 and 0·18. Values of other parameters correspond to data set #1 in Table 1. It is observed that as the value of η increases, smaller values of k^* and μ^* provide better prediction of weld dimensions, i.e. lesser values of $O(f)$. Furthermore, the values of $O(f)$ are significantly lower at $\eta=0{\cdot}13$ for any combination of k^* and μ^*. These observations are consistent with the results shown in Fig. 2.

The results plotted in Figs 2 and 3 correspond to non-dimensional heat input index N_{HI} [equation (1)] values of 300·7 and 70·5, respectively (Table 1). A comparison of Figs 2 and 3 clearly indicates a common range of the unknown parameters (Figs. 2*b* and 3*b*) even with large variation in the values of N_{HI}. Considering the fact that N_{HI} is directly linked with the amount of heat input to the substrate, the fact that η, k^* and μ^* do not show any dependence on N_{HI} requires some discussion. Although a linear relation of k^* and μ^* with a similar heat input index was reported earlier in the case of linear laser welding,[37] the same does not appear to be inherent in laser spot welding. One possible reason can be stated as the transient nature of the spot welding process in contrast to the pseudosteady state of the weld pool in linear laser weld. The melting and subsequent solidification of weld pool in the case of laser spot welding are too rapid to be influenced by the change in convective heat transport owing to the increase in laser power density (N_{HI}). A common set of optimum values of k^* and μ^* over the whole range of N_{HI} considered in the present work are therefore determined. Furthermore, the actual value of η greatly depends on the mode of laser welding and all the welds considered in the present work were fabricated in conduction mode. Therefore, a single optimum value of η for the complete range of N_{HI} considered here does not appear unrealistic.

A set of initial values of η, k^* and μ^* are necessary to start the optimisation calculations. Three measured weld pool dimensions (data set index #1, #3 and #4 in Table 1) are used to check the robustness of the proposed calculation scheme. Figures 1–3 indicate that the expression $[\partial O(f)/\partial f_i]_{i=1,3}$ does not necessarily confirm to a continuous, convex or concave type function and the solution of equation (15) may exhibit multiple local minima. To address this difficulty, the optimisation calculations are performed with a number

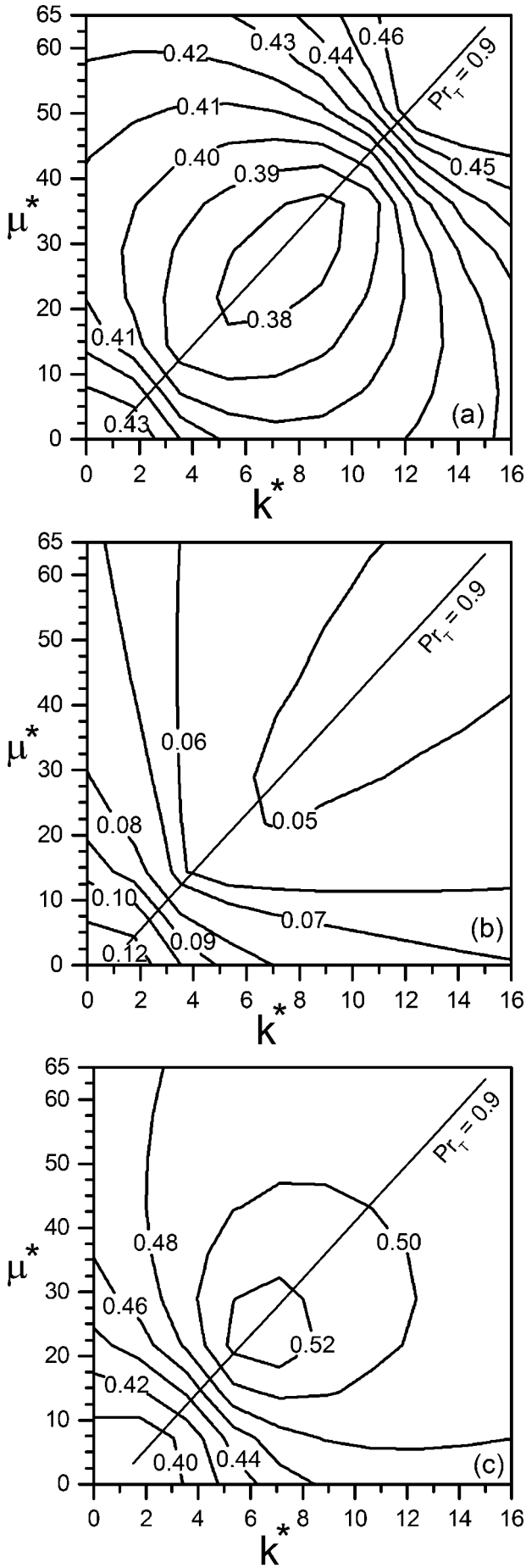

3 Influence of k^* and μ^* on $O(f)$ for absorptivity η values as *a* 0·10, *b* 0·13 and *c* 0·18: welding parameters P=1900 W, r_{b}=1·4 mm and laser on-time=5·0 s

of initial values in the ranges of 0·10–0·50, 1·0–10·0 and 1·0–40·0 for η, k^* and μ^*, respectively. Furthermore, each optimisation iteration involves a number of numerical heat transfer and fluid flow calculations for the evaluation of terms such as $[\partial O(f)/\cdot\partial f_i]_{i=1,3}$. The optimisation scheme indicated here is computationally intensive as can be appreciated from the number of numerical heat transfer and fluid flow calculations N required for one optimisation iteration is given by

$$N = (L \times M) + M \tag{18}$$

where L is the number of unknown variables and M the number of weld measurements. In equation (18), the first and second terms on the right hand side indicate the number of numerical heat transfer and fluid flow calculations required for sensitivity calculation and for testing, respectively. The optimised values of the three unknown parameters so obtained were next used for the numerical calculation of weld pool dimensions for the same data sets (#1, #3 and #4) as well as for the data sets #2, #5 and #6 (Table 1) that were not known to the optimiser.

Figure 4*a–f* presents the results of the optimisation calculations for six different sets of initially guessed values (Table 5) of the three unknown parameters, i.e. k^*, μ^* and η. These figures show that the minimum attainable value of $O(f)$ is rarely affected by the choice of the initial values. A minimum value of $O(f)$ ($\approx$0·10175) was obtained for all the six sets of initial values of the unknown parameters. The value of $O(f)$ could not be reduced below 0·10175 with various other sets of initial guesses. The results in Fig. 4*a–f* also show that the number of iterations to converge to a minimum value of $O(f)$ tends to depend on the initially guessed values. This behaviour is probably expected because $O(f)$ does not truly represent a convex type of function. For example, it required two iterations to converge to the minimum value of $O(f)$ with the first set of initially guessed values (Fig. 4*a*). Similarly, the second, fourth and fifth sets of initial guesses required three iterations while the third and sixth sets of initial guesses took four iterations to converge to the minimum value of $O(f)$. The final optimum solutions of k^*, μ^* and η were 8·12, 31·94, and 0·1326, respectively for $O(f)$ of $\sim$0·10175. The values of these parameters were nearly the same irrespective of the initial guessed values. In other words, an effective conductivity of 203 W m^{-1} K^{-1} and effective viscosity of 0·214 kg m^{-1} s^{-1} are obtained as the optimum properties while the optimum value of the absorptivity is found to be 0·1326.

The computed values of p_m^* and w_m^* using the optimised values of η, k^* and μ^* are plotted in Fig. 5 for all values of N_{HI}. A fairly satisfactory agreement is obtained between the computed and the measured weld dimensions. Values of η, k^* and μ^* estimated in the present work are consistent with their earlier approximations reported in the literature. For example, values in the range of 30–100 for both k^* and μ^* were approximated through trial and error to achieve good agreement between the computed and the measured weld dimensions.[32] When the k–ε turbulence model with a spatially variable effective viscosity was used, a maximum value of 16 for μ^* was reported to be suitable for stationary gas tungsten are (GTA) weld pool.[52] Although a slight variation of η with laser power was reported earlier based on analytical and experimental studies,[53] the estimated value of η in the present work is in good agreement with other previous works.[35] The values of η, k^* and μ^* are apparent for the specific conditions of welding considered here while a similar approach can always be adopted for other welding conditions.[36,37] Because η, k^* and μ^* are linked with p_m^* and w_m^* through the equations of conservation of mass, momentum and energy rather than through a straightforward polynomial function, local minima have been avoided by repeating the procedure with several sets of initial values. The framework presented in the present work for determining the uncertain parameters will result in enhanced reliability and is expected to significantly reduce end user's task in the numerical modelling of heat transfer and fluid flow in the weld pool.

Table 5 Sets of initial guesses for unknown parameters k^*, μ^* and η

	Set 1	Set 2	Set 3	Set 4	Set 5	Set 3	Final value
k^*	4·0	1·0	10·0	2·0	5·0	3·5	8·12
μ^*	10·0	5·0	40·0	2·0	5·0	4·5	31·94
η	0·10	0·2	0·30	0·2	0·5	0·45	0·1326

Figure 6 shows that the computed weld cross-section obtained using the optimum values of absorptivity, effective thermal conductivity and effective viscosity is in fair agreement with the corresponding experimental measurements. The calculated results also show the temperature contours and the computed velocity field. The computed velocity field shows that the liquid metal is transported from the middle of the pool outwards to the periphery owing to negative temperature coefficient of surface tension. These calculated results are consistent with the typical temperature and velocity fields for laser spot welds reported in the literature.

Summary and conclusions

The optimised values of laser beam absorptivity, effective thermal conductivity and effective diffusivity were determined from a limited volume of experimentally measured weld dimensions. The calculation procedure involved augmentation of a multivariable optimisation scheme with a numerical heat and fluid flow model, and the combined model improved the reliability of the heat transfer calculations while eliminating the end user task of empirically adjusting the uncertain variables. The gradient based Levenberg–Marquardt optimisation technique could determine the optimum values of absorptivity, effective thermal conductivity and viscosity. When the optimum values of these parameters were used in the heat transfer and fluid flow model, accurate values of weld geometry could be predicted. The initially guessed values of unknown parameters affected the number of iterations needed for convergence but not the optimum values of the unknown parameters. The values of effective thermal conductivity and effective viscosity were found to be much higher than their corresponding molecular values. The use of the optimised values of absorptivity, effective thermal conductivity and effective viscosity resulted in good agreement between the computed and the experimentally determined fusion zone geometry without the need to adjust these parameters by trial and error.

Appendix

In order to explain the basic concept of the LM method, a simplified system involving three unknown

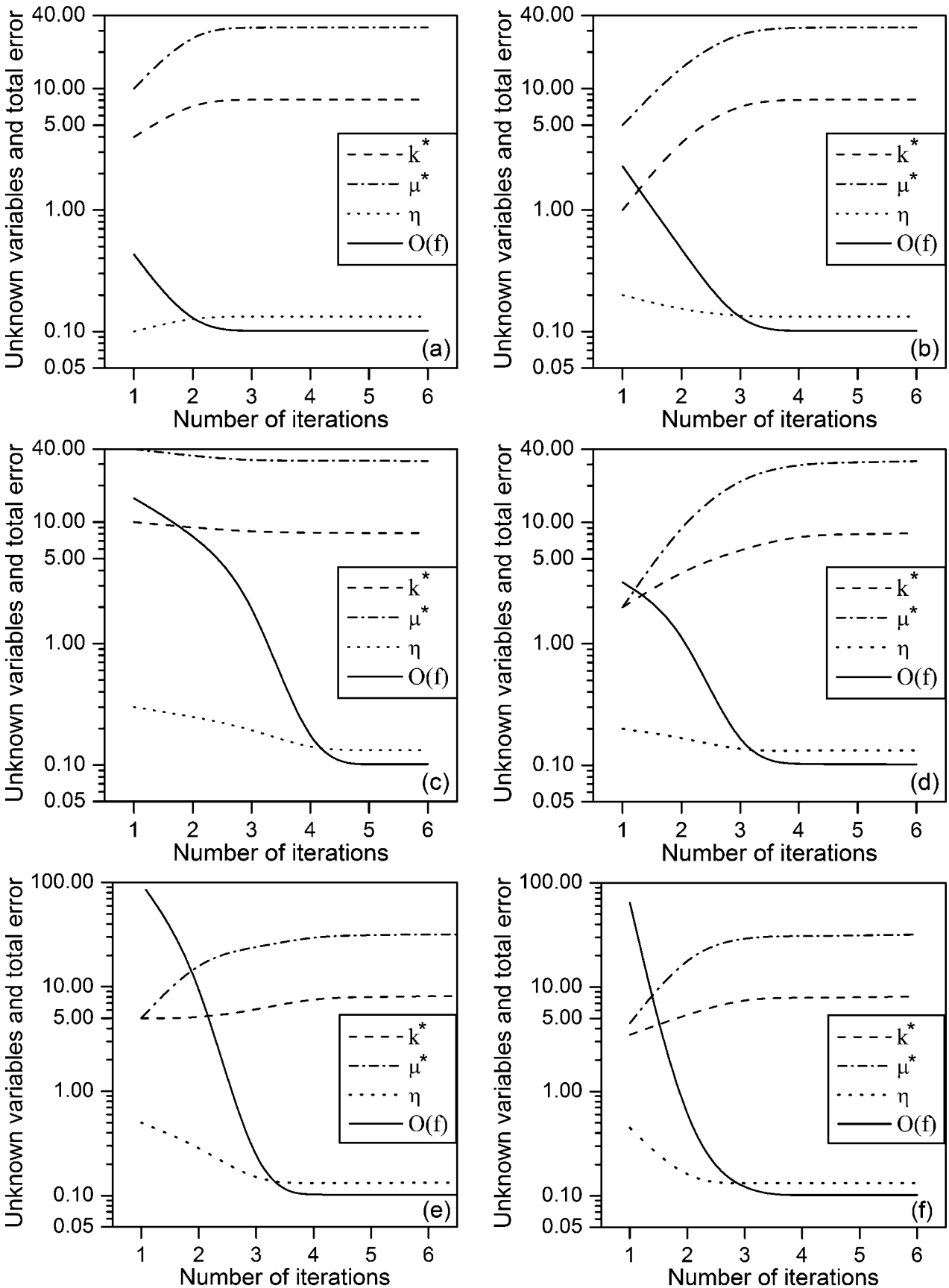

a k^*=4·0, μ^*=10·0, η=**0·1**; *b* k^*=1·0, μ^*=5·0, η=**0·2**; *c* k^*=10·0, μ^*=40·0, η=**0·3**; *d* k^*=2·0, μ^*=2·0, η=**0·2**; *e* k^*=5·0, μ^*=5·0, η=**0·5**; *f* k^*=3·5, μ^*=4·5, η=**0·45**

4 Progress of calculations with initial guessed values

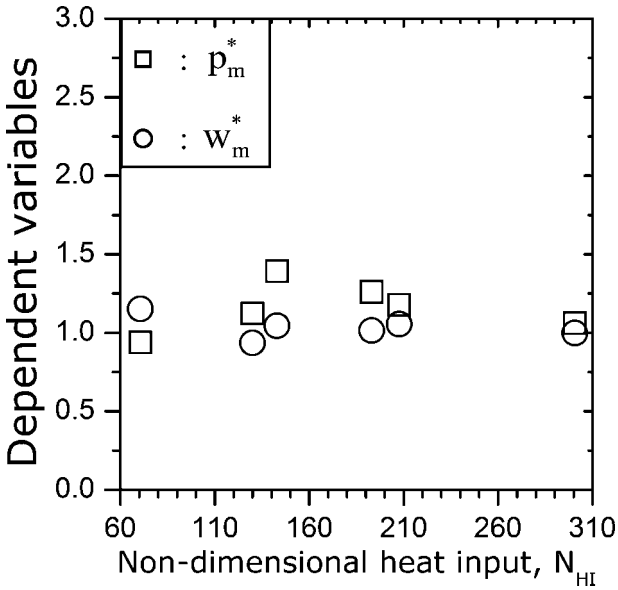

5 Computed values of p^*_m and w^*_m using optimied set of k^*, μ^* and η for all values of N_{HI}

parameters f_1, f_2 and f_3, and one dependent variable p^*_m measured under three welding conditions is considered first. Equation (13) can be written for f_1, f_2 and f_3 as

$$\sum_{m=1}^{3}\left[\left(p^*_m-1\right)\frac{\partial p^*_m}{\partial f_1}\right]=0 \tag{19}$$

$$\sum_{m=1}^{3}\left[\left(p^*_m-1\right)\frac{\partial p^*_m}{\partial f_2}\right]=0 \tag{20}$$

$$\sum_{m=1}^{3}\left[\left(p^*_m-1\right)\frac{\partial p^*_m}{\partial f_3}\right]=0 \tag{21}$$

the terms, i.e. k^* and μ^* and η, do not appear explicitly in equations (19), (20) and (21). Therefore, the solution of f_1, f_2 and f_3 requires some rearrangement of those equations. The dependent variable p^*_m is next expanded using the Taylor's series expansion to explicitly contain values of increments, and f_1, f_2 and f_3. Considering two successive iterations of p^*_m and taking only the first order terms

$$\left(p^*_m\right)^{k+1}=\left(p^*_m\right)^k+\frac{\partial\left(p^*_m\right)^k}{\partial f_1}\Delta f_1^k+\frac{\partial\left(p^*_m\right)^k}{\partial f_2}\Delta f_2^k+\frac{\partial\left(p^*_m\right)^k}{\partial f_3}\Delta f_3^k \tag{22}$$

where Δf_1^k, Δf_2^k and Δf_3^k are three unknown increments corresponding to f_1, f_2 and f_3 as

$$\begin{aligned} f_1^{k+1}&=f_1^k+\Delta f_1^k\\ f_2^{k+1}&=f_2^k+\Delta f_2^k\\ f_3^{k+1}&=f_3^k+\Delta f_3^k \end{aligned} \tag{23}$$

and f_1^{k+1}, f_2^{k+1} and f_3^{k+1} correspond to the values of three unknowns after $(k+1)$th iteration. In equation (22), all other terms on the right hand side except Δf_1^k, Δf_2^k and Δf_3^k are considered to be known. Next, equations (19), (20) and (21) are rewritten replacing p^*_m by $\left(p^*_m\right)^{k+1}$ as

$$\sum_{m=1}^{3}\left\{\left[\left(p^*_m\right)^{k+1}-1\right]\frac{\left(\partial p^*_m\right)^{k+1}}{\partial f_1}\right\}=0 \tag{24}$$

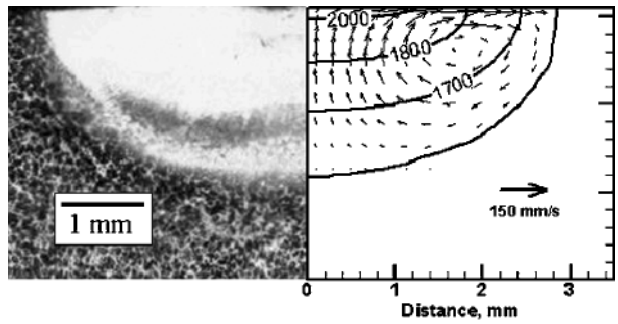

6 Computed temperature and velocity fields: length of black arrow shows magnitude of velocities and solid lines show isotherms; welding parameters P=5200 W, r_b=1·35 mm and t=15 s (N_{HI}=51·85, data set #6 in Table 1)

$$\sum_{m=1}^{3}\left\{\left[\left(p^*_m\right)^{k+1}-1\right]\frac{\left(\partial p^*_m\right)^{k+1}}{\partial f_2}\right\}=0 \tag{25}$$

$$\sum_{m=1}^{3}\left\{\left[\left(p^*_m\right)^{k+1}-1\right]\frac{\left(\partial p^*_m\right)^{k+1}}{\partial f_3}\right\}=0 \tag{26}$$

however, p^*_m equals to p^c_m/p^{obs}_m and although p^{obs}_m is a known measured value, p^c_m is to be computed using the numerical heat transfer and fluid flow calculation for a set of f_1, f_2, f_3 and other known parameters. Therefore, $\left(p^*_m\right)^{k+1}$, i.e. the value of p^*_m after $(k+1)$th iteration, is unknown because Δf_1^k, Δf_2^k and Δf_3^k are unknown. Next, substituting right hand side of equation (22) in the place of $\left(p^*_m\right)^{k+1}$, equations (24), (25) and (26) are rewritten as

$$\sum_{m=1}^{3}\left\{\frac{\left[\left(p^*_m\right)^k+\frac{\partial\left(p^*_m\right)^k}{\partial f_1}\Delta f_1^k+\frac{\partial\left(p^*_m\right)^k}{\partial f_2}\Delta f_2^k+\frac{\partial\left(p^*_m\right)^k}{\partial f_3}\Delta f_3^k-1\right]\times\partial\left[\left(p^*_m\right)^k+\frac{\partial\left(p^*_m\right)^k}{\partial f_1}\Delta f_1^k+\frac{\partial\left(p^*_m\right)^k}{\partial f_2}\Delta f_2^k+\frac{\partial\left(p^*_m\right)^k}{\partial f_3}\Delta f_3^k\right]}{\partial f_1}\right\}=0 \tag{27}$$

$$\sum_{m=1}^{3}\left\{\frac{\left[\left(p^*_m\right)^k+\frac{\partial\left(p^*_m\right)^k}{\partial f_1}\Delta f_1^k+\frac{\partial\left(p^*_m\right)^k}{\partial f_2}\Delta f_2^k+\frac{\partial\left(p^*_m\right)^k}{\partial f_3}\Delta f_3^k-1\right]\times\partial\left[\left(p^*_m\right)^k+\frac{\partial\left(p^*_m\right)^k}{\partial f_1}\Delta f_1^k+\frac{\partial\left(p^*_m\right)^k}{\partial f_2}\Delta f_2^k+\frac{\partial\left(p^*_m\right)^k}{\partial f_3}\Delta f_3^k\right]}{\partial f_2}\right\}=0 \tag{28}$$

$$\sum_{m=1}^{3}\left\{\frac{\left[\left(p^*_m\right)^k+\frac{\partial\left(p^*_m\right)^k}{\partial f_1}\Delta f_1^k+\frac{\partial\left(p^*_m\right)^k}{\partial f_2}\Delta f_2^k+\frac{\partial\left(p^*_m\right)^k}{\partial f_3}\Delta f_3^k-1\right]\times\partial\left[\left(p^*_m\right)^k+\frac{\partial\left(p^*_m\right)^k}{\partial f_1}\Delta f_1^k+\frac{\partial\left(p^*_m\right)^k}{\partial f_2}\Delta f_2^k+\frac{\partial\left(p^*_m\right)^k}{\partial f_3}\Delta f_3^k\right]}{\partial f_3}\right\}=0 \tag{29}$$

neglecting higher order differentials, e.g. $\frac{\partial}{\partial f_1}\left[\frac{\partial\left(p^*_m\right)^k}{\partial f_1}\Delta f_1^k\right]$ etc., equations (27), (28) and (29) are further simplified as

$$\sum_{m=1}^{3}\left\{\left[\left(p^*_m\right)^k+\frac{\partial\left(p^*_m\right)^k}{\partial f_1}\Delta f_1^k+\frac{\partial\left(p^*_m\right)^k}{\partial f_2}\Delta f_2^k+\frac{\partial\left(p^*_m\right)^k}{\partial f_3}\Delta f_3^k-1\right]\frac{\partial\left(p^*_m\right)^k}{\partial f_1}\right\}=0 \tag{30}$$

$$\sum_{m=1}^{3}\left\{\left[\left(p^*_m\right)^k+\frac{\partial\left(p^*_m\right)^k}{\partial f_1}\Delta f_1^k+\frac{\partial\left(p^*_m\right)^k}{\partial f_2}\Delta f_2^k+\frac{\partial\left(p^*_m\right)^k}{\partial f_3}\Delta f_3^k-1\right]\frac{\partial\left(p^*_m\right)^k}{\partial f_2}\right\}=0 \tag{31}$$

$$\sum_{m=1}^{3}\left\{\left[\left(p^*_m\right)^k+\frac{\partial\left(p^*_m\right)^k}{\partial f_1}\Delta f_1^k+\frac{\partial\left(p^*_m\right)^k}{\partial f_2}\Delta f_2^k+\frac{\partial\left(p^*_m\right)^k}{\partial f_3}\Delta f_3^k-1\right]\frac{\partial\left(p^*_m\right)^k}{\partial f_3}\right\}=0 \tag{32}$$

equations (30), (31) and (32) are next rearranged as

$$\sum_{m=1}^{3}\left[\frac{\partial\left(p_m^*\right)^k}{\partial f_1}\frac{\partial\left(p_m^*\right)^k}{\partial f_1}\right]\Delta f_1^k+\sum_{m=1}^{3}\left[\frac{\partial\left(p_m^*\right)^k}{\partial f_1}\frac{\partial\left(p_m^*\right)^k}{\partial f_2}\right]\Delta f_2^k+\sum_{m=1}^{3}\left[\frac{\partial\left(p_m^*\right)^k}{\partial f_1}\frac{\partial\left(p_m^*\right)^k}{\partial f_3}\right]\Delta f_3^k=-\sum_{m=1}^{3}\left\{\frac{\partial\left(p_m^*\right)^k}{\partial f_1}\left[\left(p_m^*\right)^k-1\right]\right\} \quad (33)$$

$$\sum_{m=1}^{3}\left[\frac{\partial\left(p_m^*\right)^k}{\partial f_2}\frac{\partial\left(p_m^*\right)^k}{\partial f_1}\right]\Delta f_1^k+\sum_{m=1}^{3}\left[\frac{\partial\left(p_m^*\right)^k}{\partial f_2}\frac{\partial\left(p_m^*\right)^k}{\partial f_2}\right]\Delta f_2^k+\sum_{m=1}^{3}\left[\frac{\partial\left(p_m^*\right)^k}{\partial f_2}\frac{\partial\left(p_m^*\right)^k}{\partial f_3}\right]\Delta f_3^k=-\sum_{m=1}^{3}\left\{\frac{\partial\left(p_m^*\right)^k}{\partial f_2}\left[\left(p_m^*\right)^k-1\right]\right\} \quad (34)$$

$$\sum_{m=1}^{3}\left[\frac{\partial\left(p_m^*\right)^k}{\partial f_3}\frac{\partial\left(p_m^*\right)^k}{\partial f_1}\right]\Delta f_1^k+\sum_{m=1}^{3}\left[\frac{\partial\left(p_m^*\right)^k}{\partial f_3}\frac{\partial\left(p_m^*\right)^k}{\partial f_2}\right]\Delta f_2^k+\sum_{m=1}^{3}\left[\frac{\partial\left(p_m^*\right)^k}{\partial f_3}\frac{\partial\left(p_m^*\right)^k}{\partial f_3}\right]\Delta f_3^k=-\sum_{m=1}^{3}\left\{\frac{\partial\left(p_m^*\right)^k}{\partial f_3}\left[\left(p_m^*\right)^k-1\right]\right\} \quad (35)$$

equations (33), (34) and (35) can be expressed in matrix form as

$$[S]\left\{\Delta f^k\right\}=-\left\{S^*\right\} \quad (36)$$

where

$$[S]=\begin{bmatrix}S_{11}&S_{12}&S_{13}\\S_{21}&S_{22}&S_{23}\\S_{31}&S_{32}&S_{33}\end{bmatrix} \quad (37)$$

$$=\begin{bmatrix}\sum_{m=1}^{3}\frac{\partial\left(p_m^*\right)^k}{\partial f_1}\frac{\partial\left(p_m^*\right)^k}{\partial f_1}&\sum_{m=1}^{3}\frac{\partial\left(p_m^*\right)^k}{\partial f_1}\frac{\partial\left(p_m^*\right)^k}{\partial f_2}&\sum_{m=1}^{3}\frac{\partial\left(p_m^*\right)^k}{\partial f_1}\frac{\partial\left(p_m^*\right)^k}{\partial f_3}\\\sum_{m=1}^{3}\frac{\partial\left(p_m^*\right)^k}{\partial f_2}\frac{\partial\left(p_m^*\right)^k}{\partial f_1}&\sum_{m=1}^{3}\frac{\partial\left(p_m^*\right)^k}{\partial f_2}\frac{\partial\left(p_m^*\right)^k}{\partial f_2}&\sum_{m=1}^{3}\frac{\partial\left(p_m^*\right)^k}{\partial f_2}\frac{\partial\left(p_m^*\right)^k}{\partial f_3}\\\sum_{m=1}^{3}\frac{\partial\left(p_m^*\right)^k}{\partial f_3}\frac{\partial\left(p_m^*\right)^k}{\partial f_1}&\sum_{m=1}^{3}\frac{\partial\left(p_m^*\right)^k}{\partial f_3}\frac{\partial\left(p_m^*\right)^k}{\partial f_2}&\sum_{m=1}^{3}\frac{\partial\left(p_m^*\right)^k}{\partial f_3}\frac{\partial\left(p_m^*\right)^k}{\partial f_3}\end{bmatrix}$$

and

$$\left\{S^*\right\}=\begin{Bmatrix}S_1^p\\S_2^p\\S_3^p\end{Bmatrix}=\begin{Bmatrix}\sum_{m=1}^{3}\frac{\partial\left(p_m^*\right)^k}{\partial f_1}\left[\left(p_m^*\right)^k-1\right]\\\sum_{m=1}^{3}\frac{\partial\left(p_m^*\right)^k}{\partial f_2}\left[\left(p_m^*\right)^k-1\right]\\\sum_{m=1}^{3}\frac{\partial\left(p_m^*\right)^k}{\partial f_3}\left[\left(p_m^*\right)^k-1\right]\end{Bmatrix} \quad (38)$$

$$\left\{\Delta f^k\right\}=\begin{Bmatrix}\Delta f_1^k\\\Delta f_2^k\\\Delta f_3^k\end{Bmatrix} \quad (39)$$

therefore, equations (19), (20) and (21) are modified to equation (36) where the three unknown incremental terms Δf_1^k, Δf_2^k and Δf_3^k are explicitly defined in terms of the known quantities. The solution of Δf_1^k, Δf_2^k and Δf_3^k are used next to obtain f_1^{k+1}, f_2^{k+1} and f_3^{k+1} [equation (23)] that are employed to compute $\left(p_m^c\right)^{k+1}$ using the numerical heat transfer and fluid flow model. Next, $O(f)^{k+1}$ is calculated as

$$O(f)^{k+1}=\sum_{m=1}^{3}\left[\left(p_m^*\right)^{k+1}-1\right]^2 \quad (40)$$

values of f_1, f_2 and f_3 are assumed to reach optimum when the calculated value of $O(f)^{k+1}$ is smaller than a predefined small number. For the two dependent variables p_m^* and w_m^*, and any M number of independent measurements, equation (37) is modified as

$$[S]=\begin{bmatrix}S_{11}&S_{12}&S_{13}\\S_{21}&S_{22}&S_{23}\\S_{31}&S_{32}&S_{33}\end{bmatrix} \quad (41)$$

where

$$S_{ij}=\sum_{m=1}^{M}\left[\frac{\partial\left(p_m^*\right)^k}{\partial f_i}\frac{\partial\left(p_m^*\right)^k}{\partial f_j}+\frac{\partial\left(w_m^*\right)^k}{\partial f_i}\frac{\partial\left(w_m^*\right)^k}{\partial f_j}\right] \quad (42)$$

for $i,j=1$ to 3

equation (38) will be modified as

$$\left\{S^*\right\}=\begin{Bmatrix}S_1^{pw}\\S_2^{pw}\\S_3^{pw}\end{Bmatrix}= \quad (43)$$

$$\begin{Bmatrix}\sum_{m=1}^{M}\left(\frac{\partial\left(p_m^*\right)^k}{\partial f_1}\left(\left(p_m^*\right)^k-1\right)+\frac{\partial\left(w_m^*\right)^k}{\partial f_1}\left(\left(w_m^*\right)^k-1\right)\right)\\\sum_{m=1}^{M}\left(\frac{\partial\left(p_m^*\right)^k}{\partial f_2}\left(\left(p_m^*\right)^k-1\right)+\frac{\partial\left(w_m^*\right)^k}{\partial f_2}\left(\left(w_m^*\right)^k-1\right)\right)\\\sum_{m=1}^{M}\left(\frac{\partial\left(p_m^*\right)^k}{\partial f_3}\left(\left(p_m^*\right)^k-1\right)+\frac{\partial\left(w_m^*\right)^k}{\partial f_3}\left(\left(w_m^*\right)^k-1\right)\right)\end{Bmatrix}$$

equations (23) and (39) do not change because the number of unknown parameters remains three. Furthermore, the sensitivity terms such as $\partial\left(p_m^*\right)^k/\partial f_i$ or $\partial\left(w_m^*\right)^k/\partial f_i$ (for i=1 to 3) in equation (36) often tend to be very small as the values of the unknown parameters f_1, f_2 and f_3 move close to the optimum. As a result, the matrix $[S]$ tends to become singular. To avoid numerical instability, equation (36) is further modified following LM method as

$$([S]+\lambda\mathbf{I})\quad\left\{\Delta f^k\right\}=-\left\{S^*\right\} \quad (44)$$

where λ is a scalar damping coefficient, usually $\sim$0·001, and $\mathbf{I}$ is a diagonal matrix given by[42]

$$\mathbf{I}=\begin{bmatrix}S_{11}&0&0\\0&S_{22}&0\\0&0&S_{33}\end{bmatrix} \quad (45)$$

the product $\lambda\mathbf{I}$ in equation (44) ensures that the left hand term in equation (44) will remain non-zero even though the determinant of the matrix $[S]$ is 0. The value of λ is usually increased or decreased by a factor of 10 as the value of the objective function in subsequent iterations

increases or decreases. This, in effect, ensures the reduction or enhancement in step size as the solution respectively tends to diverge or converge. The algorithm of the complete procedure using LM method can be presented as follows

Step 1: guess initial values (e.g. kth) of unknown variables set, $\{f_i^k\}$ for $i=1,3$ from equation (12).

Step 2: choose initial value of damping factor λ.

Step 3: compute the value of the objective function $O(f^k)$ from equation (11).

Step 4: solve for the set of unknown increments $\{\Delta f_i^k\}$ for $i=1,3$ from equation (44).

Step 5: compute $\{f_i^{k+1}\}$ for $i=1, 3$ from equation (23).

Step 6: compute $O(f^{k+1})$ from equation (11).

Step 7: if $O(f^{k+1}) \geqslant O(f^k)$, set $\lambda=10\ \lambda$; reject $\{f_i^{k+1}\}$; go back to step 4.

Step 8: if $O(f^{k+1}) < O(f^k)$, set $\lambda=0{\cdot}1\ \lambda$.

Step 9: exit if $O(f^{k+1}) - O(f^k) \leqslant \varepsilon_1$ and $\{f_i^{k+\S}\} - \{f_i^k\} \leqslant \varepsilon_2$; or go back to step 4. ε_1 and ε_2 are two small, predefined numbers.

Acknowledgements

The work was supported by a grant from the US Department of Energy, Office of Basic Energy Sciences, Division of Materials Sciences under grant number DE-FGO2-01ER45900. The authors appreciate critical comments on the work from Mr S. Mishra, Ms Xiuli He and Mr A. Kumar.

References

1. K. Hong, D. C. Weckmann, A. B. Strong and W. Zheng: *Sci. Technol. Weld. Join.*, 2003, **8**, (5), 313–324.
2. W. Pitscheneder, T. Debroy, K. Mundra and R. Ebner: *Weld. J.*, 1996, **75**, (3), 71s–80s.
3. S. Kou and H. Y. Wang: *Metall. Trans. A*, 1986, **17A**, (12), 2265–2270.
4. A. De and T. Debroy: *Weld. J.*, 2005, **84**, (7), 101s–112s.
5. S. Mishra and T. Debroy: *J. Phys. D*, 2005, **38**, 2977–2985.
6. S. Mishra and T. Debroy: *J. Appl. Phys.*, 2005, **98**, 044902.
7. A. De, C. A. Walsh, S. K. Maiti and H. K. D. H. Bhadeshia: *Sci. Technol. Weld. Join.*, 2003, **8**, (6), 391–399.
8. W. Zhang, T. Debroy and J. W. Elmer: *Sci. Technol. Weld. Join.*, 2005, **10**, (5), 574–582.
9. W. Zhang, T. Debroy, T. A. Palmer and J. W. Elmer: *Acta Mater.*, 2005, **53**, (16), 4441–4453.
10. A. Kumar, S. Mishra, J. W. Elmer and T. Debroy: *Metall. Mater. Trans. A*, 2005, **36A**, 15–22.
11. J. W. Elmer, T. A. Palmer, S. S. Babu, W. Zhang and T. Debroy: *J. Appl. Phys.*, 2004, **95**, 8327–8337.
12. J. W. Elmer, T. A. Palmer, S. S. Babu, W. Zhang and T. Debroy: *Weld. J.*, 2004, **83**, (9), 244s–253s.
13. J. W. Elmer, T. A. Palmer, W. Zhang, B. Wood and T. Debroy: *Acta Mater.*, 2003, **51**, (12), 3333–3349.
14. S. Mishra and T. Debroy: *Acta Mater.*, 2004, **52**, (5), 1183–1192.
15. S. Mishra and T. Debroy: *J. Phys. D: Appl. Phys.*, 2004, **37**, 2191–2196.
16. T. Hong, W. Pitscheneder and T. Debroy: *Sci. Technol. Weld. Join.*, 1998, **3**, (1), 33–41.
17. T. Hong and T. Debroy: *Metall. Mater. Trans. B*, 2003, **34B**, 267–269.
18. T. Hong and T. Debroy: *Ironmak. Steelmak.*, 2001, **28**, (6), 450–454.
19. S. Mishra, S. Chakraborty and T. Debroy: *J. Appl. Phys.*, 2005, **97**, 94912–94920.
20. X. He, T. Debroy and P. Fuerschbach: *J. Appl. Phys.*, 2004, **96**, 4547–4555.
21. H. Zhao and T. Debroy: *Metall. Mater. Trans. B*, 2001, **32B**, 163–172.
22. T. A. Palmer and T. Debroy: *Metall. Mater. Trans. B*, 2000, **31B**, 1371–1385.
23. K. Mundra, J. M. Blackburn and T. Debroy: *Sci. Technol. Weld. Join.*, 1997, **2**, (4), 174–184.
24. X. He, J. Elmer and T. Debroy: *J. Appl. Phys.*, 2005, **97**, 84909–84917.
25. W. Zhang, G. G. Roy, J. W. Elmer and T. Debroy: *J. Appl. Phys.*, 2003, **93**, (5), 3022–3033.
26. A. Kumar, W. Zhang and T. Debroy: *J. Phys. D*, 2005, **38**, 118–126.
27. A. Kumar and T. Debroy: *J. Phys. D*, 2005, **38**, 127–134.
28. W. Zhang, C. L. Kim and T. Debroy: *J. Appl. Phys.*, 2004, **95**, 5210–5219.
29. W. Zhang, C. L. Kim and T. Debroy: *J. Appl. Phys.*, 2004, **95**, 5220–5229.
30. A. Kumar and T. Debroy: *Int. J. Heat Mass Trans.*, 2004, **47**, (26), 5793–5806.
31. T. Debroy and S. Kou: in 'Welding handbook', 9th edn, Vol. 1, Chapter 3, 87–113; 2001, Miami, FL, American Welding Society.
32. R. T. C. Choo and J. Szekely: *Weld. J.*, 1994, **73**, (2), 25s–31s.
33. P. G. Jonsson, J. Szekely, R. T. C. Choo and T. P. Quinn: *Modell. Simul. Mater. Sci. Eng.*, 1994, **2**, (5), 995–1016.
34. Z. Yang and T. Debroy: *Metall. Mater. Trans. B*, 1999, **30B**, 483–493.
35. W. Pitscheneder: 'Contribution to the understanding and optimization of laser surface alloying', PhD thesis, University of Leoben, Austria, 2001.
36. A. De and T. Debroy: *J. Phys. D: Appl. Phys.*, 2004, **37**, (1), 140–150.
37. A. De and T. Debroy: *J. Appl. Phys.*, 2004, **95**, (9), 5230–5240.
38. Y. F. Hsu, B. Rubinsky and K. Mahin: *J. Heat Trans. Trans. ASME*, 1986, **108**, (4), 734–741.
39. J. V. Beck: Proc. 5th Int. Conf. on 'Modeling of casting, welding and advanced solidification processes', (ed. M. Rappaz *et al.*), 503–514; 1991, Warrendale, PA, TMS.
40. M. Rappaz, J. L. Desbiolles, J. M. Drezet, C. A. Gandin, A. Jacot and P. Thevoz: Proc. 7th Int. Conf. on 'Modeling of casting, welding and advanced solidification processes', (ed. M. Cross *et al.*), 449–457; 1995, Warrendale, PA, TMS.
41. R. W. Fonda and S. G. Lambrakos: *Sci. Technol. Weld. Join.*, 2002, **7**, (3), 177–181.
42. V. A. Karkhin, V. V. Plochikhine and H. W. Bergmann: *Sci. Technol. Weld. Join.*, 2002, **7**, (4), 224–231.
43. S. V. Patankar: 'Numerical heat transfer and fluid flow'; 1992, New York, McGraw-Hill.
44. A. Kumar and T. Debroy: *J. Appl. Phys.*, 2003, **94**, (2), 1267–1277.
45. V. R. Voller and C. Prakash: *Int. J. Heat Mass Trans.*, 1987, **30**, 1709–1719.
46. A. D. Brent, V. R. Voller and K. J. Reid: *Numer. Heat Trans.*, 1988, **13**, 297–318.
47. K. Mundra, T. Debroy and M. K. Kelkar: *Numer. Heat Trans. A*, 1996, **29**, 115–129.
48. J. V. Beck and K. J. Arnold: 'Parameter estimation in engineering and science'; 1977, New York, Wiley International.
49. J. V. Beck, B. Blackwell and C. R. Clair, Jr: 'Inverse heat conduction – ill posed problems'; 1985, New York, Wiley International.
50. O. M. Alifanov: 'Inverse heat transfer problems'; 1994, Berlin, Springer-Verlag.
51. M. N. Ozisik and H. R. B. Orlande: 'Inverse heat transfer'; 2000, New York, Taylor & Francis Inc.
52. K. Hong, D. C. Weckmann, A. B. Strong and W. Zheng: *Sci. Technol. Weld. Join.*, 2002, **7**, (5), 125–136.
53. P. W. Fuerschbach: *Weld. J.*, 1996, **75**, (1), 24s–34s.